NeWater

PROTOTYPE OF A CATCHMENT-SCALE HYDROLOGICAL MODEL AND CLIMATE SCENARIOS

- Application of the Variable Infiltration Capacity model to the Rhine basin -

Deliverable 2.2.4

Report of the NeWater project -
New Approaches to Adaptive Water Management under Uncertainty

www.newater.info

Title	Prototype of a catchment-scale hydrological model and climate scenarios: Application of the Variable Infiltration Capacity model to the Rhine basin
Purpose	Reporting the application of the water balance model VIC (Variable Infiltration Capacity) to the Rhine basin, and providing a manual for application of the model to other river basins.
Filename	Deliverable_D2.2.4_VIC_report.pdf
Authors	Ruud Hurkmans, Wilco Terink and Remko Uijlenhoet
Document history	
Current version.	
Changes to previous version.	
Date	08/02/08
Status	Final
Target readership	
General readership	
Correct reference	

Ruud Hurkmans, Wilco Terink and Remko Uijlenhoet
Hydrology and Quantitative Water Management, Wageningen University

January 2008

Prepared under contract from the European Commission

Contract no 511179 (GOCE)
Integrated Project in
PRIORITY 6.3 Global Change and Ecosystems
in the 6th EU framework programme

Deliverable title: Prototype of a catchment-scale hydrological model and climate scenarios
Deliverable no. : **2.2.4**
Due date of deliverable: Month 36
Actual submission date: **8**-2-2008
Start of the project: January 2005
Duration: 4 years

Executive summary

The report describes the application and calibration of a distributed hydrological model (the Variable Infiltration Capacity (VIC) model) to the Rhine basin. The VIC-model is a land surface model that is designed for simulating interactions between land surface and atmosphere. Therefore, it solves the fully coupled water-and energy balance, leading to a more realistic partitioning of rainfall into runoff and evapotranspiration compared to more simple water balance models. The model also contains some parameterizations for small-scale heterogeneity which make it suitable for simulating rainfall-runoff processes.

The model was calibrated for different sub-catchments in the river basin using historical streamflow observations and atmospheric data which were downscaled with the REMO model of the Max Planck Institute for Meteorologie (MPI-M). MPI-M also provided downscaled regional climate scenarios forced by three different CO2-emission scenarios at the same resolution as the historical data (see deliverable 2.2.2a). In the near future, these regional climate scenarios will be used to generate streamflow scenarios for the River rhine by means of the VIC model. This report includes a short summary changes in precipitation and temperature over the Rhine basin up to 2050, as derived from the MPI-M regional climate scenarios.

Finally, this report contains a technical description of the application of the VIC model: data preprocessing, generation of parameter files, etc. Also a manual is included for application of the VIC model to other areas, or NeWater case study basins, based on MPI-M climate scenarios for other river basins, or global datasets.

Table of contents

1 Introduction

The objective for deliverable 2.2.4 is to develop a prototype of a catchment-scale distributed hydrological model, coupled with climate ensembles. This tool will subsequently be used to evaluate effects of climate change on the hydrological regime in the Rhine basin, and to assess the associated uncertainty in climate input and model. The model that is described below and was developed in this framework is based on the Variable Infiltration Capacity (VIC; http://www.hydro.washington.edu/Lettenmaier/Models/VIC/VIChome.html) model [Liang et al., 1994, 1996; Liang and Xie, 2001]. VIC is a land surface model (LSM), designed to simulate the interactions between land surface and atmosphere in climate models, but it has often been applied for hydrological purposes (e.g., Nijssen et al., 1997, 2001 and Wood et al, 2005) with generally good results. Moreover, previous research in this framework (Hurkmans et al., 2008), showed that LSMs like VIC have advantages over more simple water balance models that are usually used in climate assessment studies.

This document describes VIC and how it is applied to the Rhine basin. Partly, this was already published in Hurkmans et al., (2008), and therefore parts of the following have been modified from this paper. Together with this report, an archive file is supplied, containing everything needed to use VIC, except the climate scenarios themselves, which require a large amount of disk storage space (100 years of one scenario is approximately 148 GB). They can be downloaded from the website of the Max Planck Institute (result of deliverable 2.2.2). Some preprocessing is required for use with VIC, which is described in the remainder of this document.

2. Model description

VIC is a variable-layer soil-vegetation-atmosphere transfer (SVAT) scheme for general and regional circulation and weather prediction models. Typically, it is applied at relatively coarse resolutions, with pixel sizes in the order of tens of square kilometers. In the left part of Figure 1 all processes and fluxes taken into account in VIC are shown. To account for heterogeneity at smaller scales, each pixel is divided into several patches based on land cover type. All equations of the water and energy balances are then solved for each patch separately. Besides, within each patch, several elevation classes are assigned based on a high-resolution digital terrain model. Temperatures are then lapsed according to elevation, as is the portioning between snow and rain. The most distinguishing aspect of VIC in comparison with other land surface models is its variable infiltration capacity curve, which is also designed to account for sub-grid scale heterogeneity. It is described by:

$$I = I_m \left[1 - (1 - A)\right]^{1/\beta} \qquad (1)$$

where I and I_m are the infiltration capacity and maximum infiltration capacity, respectively. A is the fraction of an area for which the infiltration capacity is less than I and β is a shape parameter. Drainage from the upper to the lower layers is assumed to be driven by gravity only, using the Brooks and Corey [1964] relationship to estimate hydraulic conductivity. Baseflow is modeled following the ARNO model formulation [Todini, 1996]. The relation between soil moisture in the lowest layer and

base flow is shown in Figure 1 as 'Baseflow curve'. The parameters in that curve and, as well as depths of the soil layers, are typically used for model calibration [e.g., Lohmann et al., 1998a]. See Section 4 for more details about model calibration. When snow is present on the ground, the model is coupled with a two layer energy and mass-balance model. Snow can also be intercepted by the canopy, melt from the canopy snow pack is simulated using a simplified energy balance model. VIC can operate in two modes: in the energy balance mode, the energy balance is solved iteratively to obtain the surface temperature, whereas in the water balance mode, surface temperature is assumed equal to air temperature. In both modes, potential evapotranspiration is calculated using the Penman-Monteith equation. In the energy balance mode, a time step of 3 hours is used, in correspondence with availability of forcing data, whereas in water balance mode the model is integrated at a daily time step. Therefore simulation times are drastically reduced compared to the full mode.

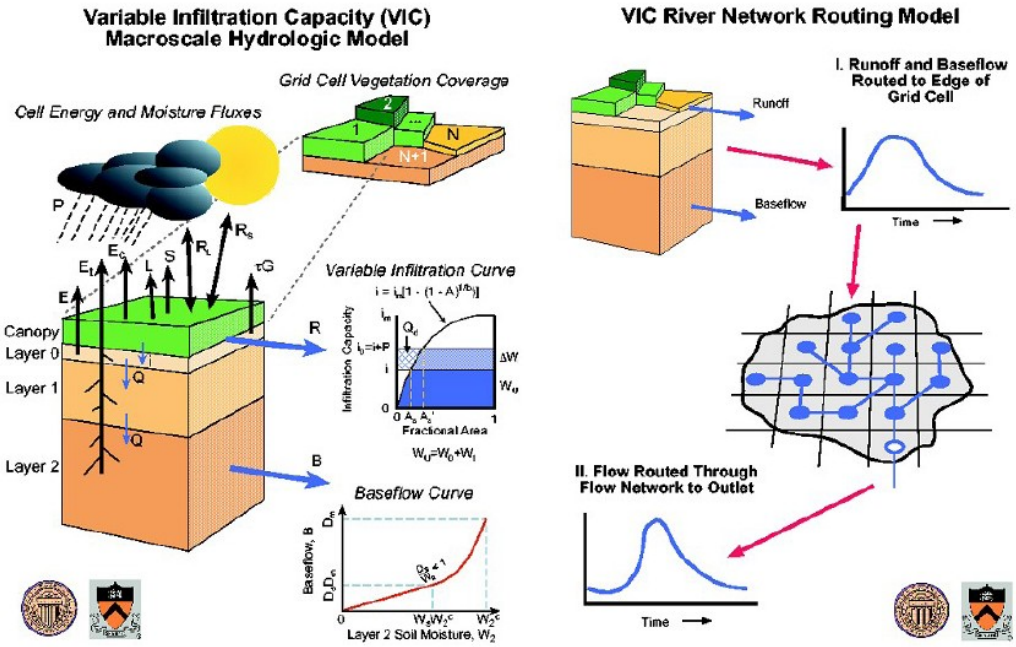

Figure 1. Schematics showing the processes and parameterizations in VIC (left) and the routing model (right).

Routing of surface runoff and base flow from all models is done by the algorithm developed by Lohmann et al. [1996], which has been applied in combination with VIC by Lohmann et al. [1998a, b]. The sum of base flow and runoff from the models is convoluted with a normalized impulse response function, based on the linearized St. Venant equation, assuming that water from each grid cell flows into the channel in the steepest direction to one of its eight neighbors, as is shown in the right part of Figure 1.

3. Data

For simulation, VIC needs information about soil types, land cover and climate. The first two are static, the latter needs to be supplied every time step. For the Rhine basin, soil type information is obtained from sand and clay percentage maps from the FAO

datasets (Reynolds et al., 2000), while land cover data are obtained from the European land cover database PELCOM (Mucher et al., 2000), which has a spatial resolution of 1 km. Climate data is described in the section 3.1. These data may not be applicable when the model is applied to other areas of the world. Section 5.3 provides sources of alternative/global datasets and some information about how preprocessing for the VIC model should be carried out.

3.1 Atmospheric data

Climate scenarios are provided by the Max Planck Institut fur Meteorologie, Hamburg, Germany (MPI-M). They cover the Rhine basin at a spatial resolution of 0.088 degrees and span the period of 2000-2100 at an hourly resolution. The scenarios are based on data from the General Circulation Model (ECHAM4) and downscaling was carried out at MPI-M using the regional climate model REMO [Jacob, 2001]. To evaluate the performance of the VIC model, a similar dataset, spanning the years 1993-2003 was created based on ERA15 reanalysis data (http://www.ecmwf.int/research/era/). This dataset will be referred to as ERA15d hereafter. In Figure 2 monthly climatologies of the seven variables that were used to force VIC, i.e., precipitation, temperature, specific humidity, surface pressure, incoming longwave and shortwave radiation and windspeed, are shown. To compare this data to observations, an additional meteorological dataset is used from the International Commission for the Hydrology of the Rhine basin (CHR), referred to as CHR hereafter. This dataset contains daily values of precipitation and temperature and is based on observations from 36 stations throughout the basin [Sprokkereef , 2001b]. Temperature and precipitation for the years present in both datasets (1993 through 1995) are also shown in Figure 2.

Climate scenario data can be requested from MPI-M. Information about how to get access (username and password) is located at:
http://www.mad.zmaw.de/projects-at-md/sg-adaptation/links-to-other-regional-model-data/remouba-project/

When login-information is obtained, the data can be downloaded through this website:
http://cera-www.dkrz.de/WDCC/ui/Index.jsp.

Note that not all data can be downloaded at the same time (i.e., in one file). We downloaded data in blocks of 5 years (corresponding to about 2.2 GB), to avoid downloadable file-size limits from web-browsers.

As was mentioned before, scenarios consist of downscaled ECHAM data, where ECHAM is forced by three different carbon emission scenarios that were defined by IPCC in the Special Report on Emission Scenarios (SRES; http://www.grida.no/climate/ipcc/emission/) . The three scenarios that were used for the REMO climate scenarios were, ranging from optimistic to pessimistic, B1, A1B and A2. For more information about their characteristics, see the SRES report. All scenarios span a period from 2001 to 2100 at an hourly base. Many variables are available, but they are not exactly identical to the seven variables required b VIC. There fore 10 variables are downloaded and, in the preprocessing step, converted to the seven variables required by VIC. The ten variables to be downloaded are listed in Table 1.

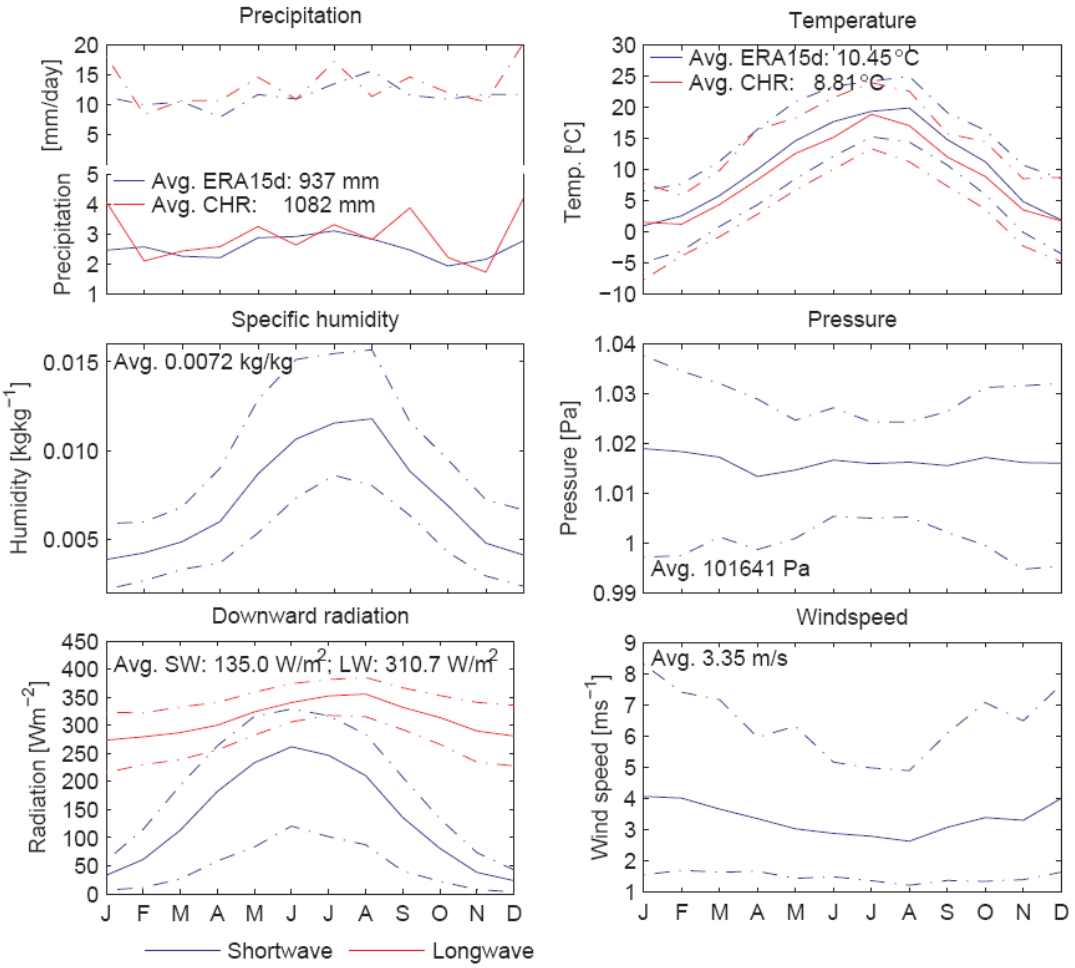

Figure 2. Climatologies of seven atmospheric variables required to run VIC in the historic dataset (1993-2003). Average values (solid lines), as well as maximum and minimum values are shown (dashed lines). For precipitation and temperature, also the CHR dataset is shown for comparison.

Table 1. Variables to be downloaded from the REMO climate scenario dataset with corresponding codes and units), to be able to obtain all required VIC variables.

Variable	**REMO code**	**Units**
Convective precipitation	APRC	mm (per timestep)
Stratiform precipitation	APRL	mm (per timestep)
Surface air pressure	PSRED	Pa
Specific humidity	QDB	kg kg^{-1}
Upward solar radiation	SRADSU	W m^{-2}
Net solar radiation	SRADS	W m^{-2}

Upward thermal radiation	TRADSU	W m^{-2}
Net thermal radiation	TRADS	W m^{-2}
2-m. air temperature	TEMP2	K
10-m. wind speed	WIND10	m s^{-1}

3.2. Preprocessing of atmospheric data

Climate scenarios as downloaded from the website are not directly usable in VIC for three reasons. First, REMO does not provide exactly the same variables that VIC requires (see Table 1). Second, REMO provides data at a hourly timestep, however, VIC only requires 3 hourly input data. To reduce data storage sizes, therefore, data are aggregated to 3-hourly. Third, the data in REMO is projected onto a rotated grid to minimize deformation of grid cells in the area under consideration. Therefore, REMO scenarios need to be preprocessed. A C-program (REMO_preprocessing) is provided in the "forcingdata_preprocessing" directory to perform this preprocessing.

3.3. Preliminary analyses of climate scenarios

Downloading the REMO Climate Scenarios is a time taking process. Therefore, for now, only the short period 2001-2025 has been downloaded for the scenarios A2 and B1. To enable a long term analysis for one scenario, the additional period 2001-2050 has been downloaded for scenario A1B. To represent the current situation, the ERA15d dataset, spanning the years 1993-2003, described in more detail in sections 3 and 4 is used. In this report, only precipitation and temperature data is investigated. In deliverable 2.2.5 (to be produced later in 2008), the analysis will be extended to include a longer time period and all seven VIC input variables. In this study, the analysis of the REMO Climate Scenarios has been divided into two parts. The first part covers an analysis of the spatial averages for the seasons winter (months December, January, February), spring (March, April, May), summer (June, July, August) and autumn (October, November, December) for each scenario and the current situation. The second part focuses on the spatial distribution of each scenario for the same seasons used in part one. In the second part, the temporal averages should represent the same length. Therefore, the period 2015-2025 (11 years) is averaged to represent scenarios A2, A1B and B1. This length is identical to the length of the current (ERA15d) dataset. In addition, for A1B the period 2035-2045 (11years) has been analyzed.

3.3.1 Spatial averages

Precipitation analysis

Figure 3 represents the average seasonal precipitation for the ERA15d dataset, and scenarios A2, A1B and B1. In this figure also the trend line for each scenario and the

corresponding slope function is plotted. There is no trend line plotted for the current situation, because this time period is too small to plot a reasonable trend line. Therefore, the thick black line represents the average for the current situation. The trend line for the period 2001-2050 for scenario A1B is represented by the dotted blue line. For the winters in period 2001-2025, the scenarios A2 and B1 both show an increase in precipitation. Scenario B1 generates the largest amount of precipitation and has the fastest increase over time. Scenario A1B is the only scenario where the amount of precipitation is decreasing over the first 25 years, but it is still more than the current situation, as all the scenarios are. However, when the trend line for the period 2001-2050 is plotted for scenario A1B, an increase in precipitation can be seen. This increase is almost similar to the increase in precipitation of scenario A2. Also in autumn the scenarios A2 and B1 show an increase in precipitation. Both scenarios are quite similar when the rate of increase is considered, but scenario B1 is producing more precipitation in the first 25 years. The only scenario showing a decreasing trend in the first 25 years is scenario A1B. However, when the trend line is plotted for the complete period of 50 years, an increase in precipitation for scenario A1B is visible. This increase is very small, due to some extreme dry events in the period 2025-2050. In autumn, all scenarios produce more precipitation than the current situation. In spring, all the scenarios show a decrease in precipitation, except for scenario B1. Even the long and short term trend lines of scenario A1B are quite comparable to each other. For the period 2001-2025 the scenarios A1B and B1 are not that different, but some extremely low values in the period 2025-2050 cause the negative slope of scenario A1B. There is a possibility that scenario B1 also will show a negative slope if data after 2025 is known. All scenarios generate more precipitation than the current situation. In summer all scenarios show an increase in precipitation. However, when the trend line for the whole period of 50 years is plotted for scenario A1B, a decrease in precipitation over time is visible. Of course this is also possible for the other two scenarios. Scenario A1B creates the largest amount of precipitation. The largest peaks can be found in scenario B1, which suggests that this scenario has more extreme events, leading to very high seasonal averages. The B1 scenario also shows the largest increase in precipitation over time whereas scenario A2 has the smallest increase over time. In general it can be concluded that the winter, summer and autumn are getting wetter and that spring is getting dryer.

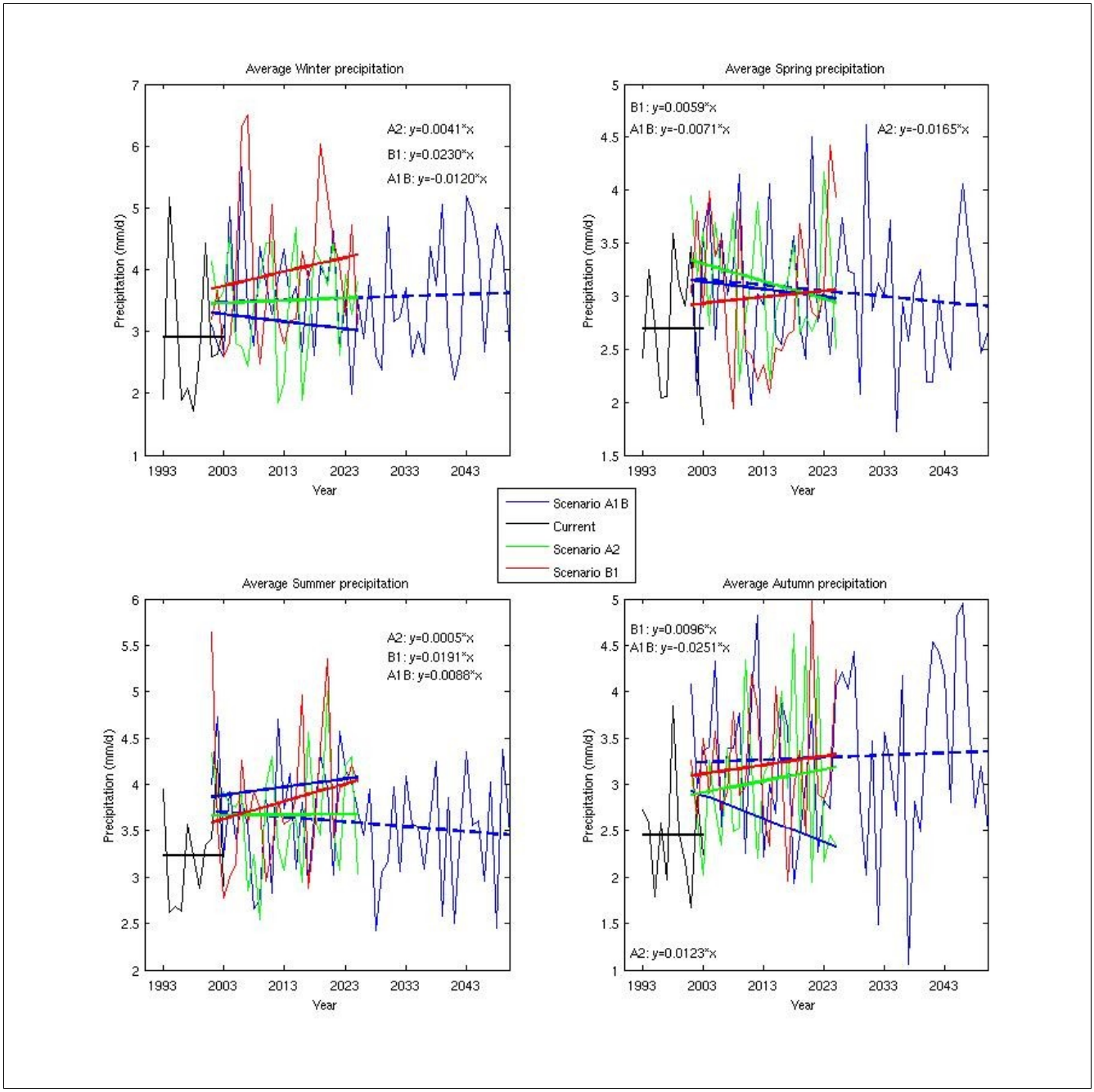

Figure 3. Average seasonal precipitation for ERA15d (1993-2003), scenario A2, scenario A1B and scenario B1.

Temperature analysis

Figure 4 represents the average seasonal temperatures for the ERA15d dataset and scenarios A2, A1B and B1, presented in a similar way. In all four subfigures, temperature in the ERA15d dataset is strikingly high compared to the scenarios. This is caused by the driving model in the creation of the scenarios: the ECHAM5 model on which the scenarios are based (section 3.1), is relatively cool compared to the ERA15 reanalysis dataset on which the ERA15d dataset is based. As is also described in section 3.1 and Hurkmans et al., (2008), the ERA15d dataset is slightly warmer than observations over the Rhine basin.

In the winter period an increase in temperature for all scenarios can be seen. The temperature in scenario B1 rises the most when compared to the other scenarios and the current situation. The slopes for the temperature increase for scenarios A1B and A2 are quite similar. In the first 25 years, scenario A2 shows a higher temperature than scenario A1B. It is, of course, not known how scenario A2 will develop after 2025. It is clear that scenario A1B will nearly continue the same trend in 2025-2050 as it used to do in 2001-2025. However, the period 2025-2050 for scenario A1B is characterized by some extremely dry and wet events, influencing the course of the trendline. An increase in temperature for all scenarios can be seen in autumn. In this season, scenario A1B develops the highest temperature. This increase is caused by some extreme events in the period 2025-2050. However, scenario B1 and A1B have the same slope and it is

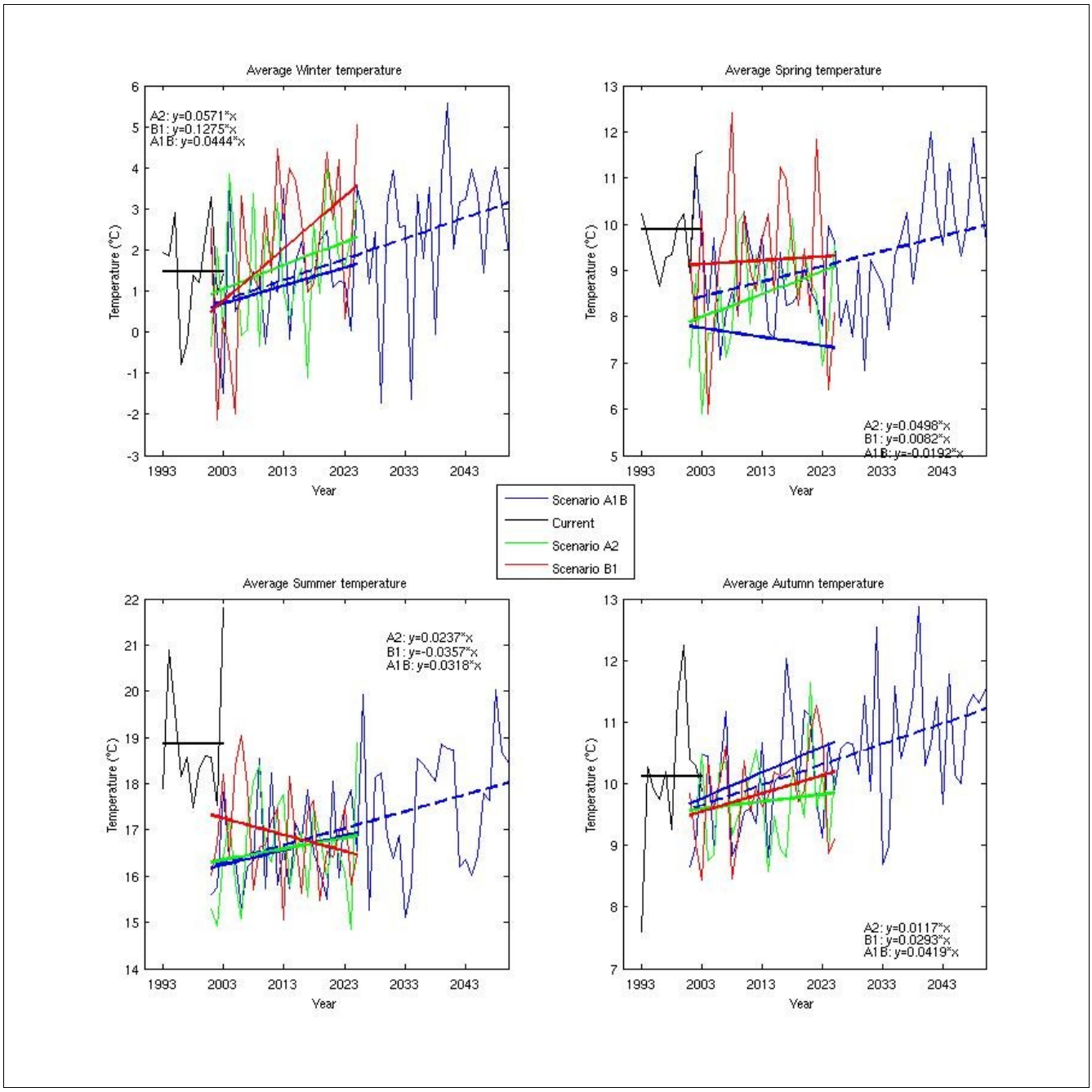

Figure 4. Average seasonal temperature for ERA15d (1993-2003), scenario A2, scenario A1B and scenario B1.

not known how scenario B1 is going to develop after 2025. It may be possible that scenario B1 also will have some extreme events after 2025 which will result in a steeper trend line. The trend line of scenario A1B for the period 2001-2025 is almost similar to the trend line for the period 2025-2050. In the first 25 years, the scenarios A2 and B1 reach nearly the same temperature increase compared to the current situation, whereas the rate of increase over time is larger for scenario B1. The little amount of data available for the current situation, combined with the extreme low and high values for this situation, creates a high average value for this situation. Therefore, it is hard to draw a good conclusion from this. In spring, the temperature increases for the scenarios A2 and B1 over the period 2001-2025. Scenario A1B is the only scenario which shows a decrease in temperature over that period. However, when the complete period 2001-2050 is taken into account, the temperature of scenario A1B shows an increase. The A2 scenario shows the steepest increase in temperature. Scenario B1 represents the highest temperature for the period 2001-2025, caused by three extremely hot periods occurring during this period. In summer, the scenarios A2 and A1B show a similar rise in temperature. It seems that the trend line of scenario A1B for the period 2001-2025 is continuing in almost the same way for the period 2025-2050. Only scenario B1 indicates a drop in temperature. However, this scenario starts with the highest temperature at the beginning of 2001-2025 and intersects the other two scenarios at 2018. The current situation for summer shows a high average temperature, as was explained in the beginning of this paragraph. In fact, the climate scenarios do not reach this high average for the plotted period. In general it can be concluded that the temperature will increase for all seasons. Scenario B1 has the largest increase in temperature in winter and is the only scenario with a decrease in temperature in summer.

3.2.2 Spatial distribution over River Rhine basin

Precipitation analysis

Figure 5 through 8 show differences in precipitation between the different scenarios and the current situation for the four seasons (winter, spring, summer, autumn) respectively. In the top right of each figure, the mean and standard deviation of the grid cells is plotted. In winter (Figure 5), for scenario A1B, two periods (2015-2025 and 2035-2045) are used. The upper left figure represents the difference between the period 2015-2025 of scenario A1B and the current situation. The grid cells all have a negative value, which means that the amount of precipitation is decreasing for this scenario in this period. The same counts for the period 2035-2045 (upper right figure). Especially in the Alps, there will be a large decrease in precipitation. Both periods of scenario A1B display an average precipitation difference of -82 mm. The scenarios A2 and B1 (lower two figures) both show an increase in precipitation in most of the Rhine Basin. The largest increase in precipitation can be found in the Alps and just north of the Alps. B1 generates more precipitation than A2 when compared with the current situation. This is also visible when the two averages of these two scenarios are compared. The largest variability can be found in scenario B1 and the smallest in scenario A1B.

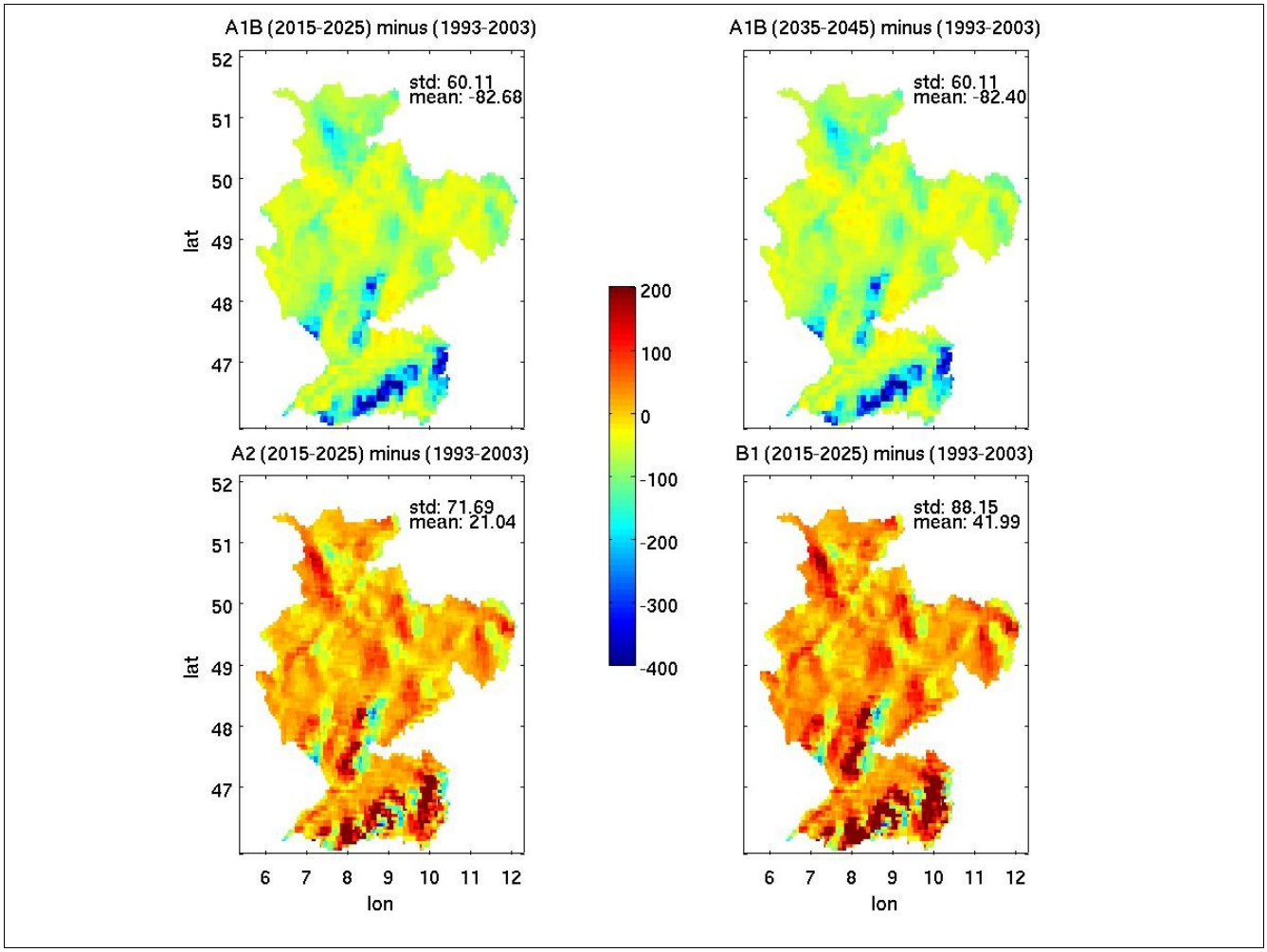

Figure 5. Difference in precipitation between climate scenarios and current situation for winter.

In spring (Figure 6), the two periods of scenario A1B (upper two figures) show a decrease in precipitation when compared with the current situation. However, the decrease is smaller than in winter (figure 5). Also the standard deviation is smaller than for the winter period. Again, the decrease in precipitation is largest in the Alps. Scenarios A2 and B1 are quite similar to each other when compared with the current situation. They both show the largest increase in precipitation in the Alps, but also the variability in the area in and around the Alps is the largest. There are also some spots in the Alps showing a decrease in precipitation. They both show a comparable average precipitation difference and standard deviation. For all scenarios, the standard deviation is significantly lower, when compared with the winter season.

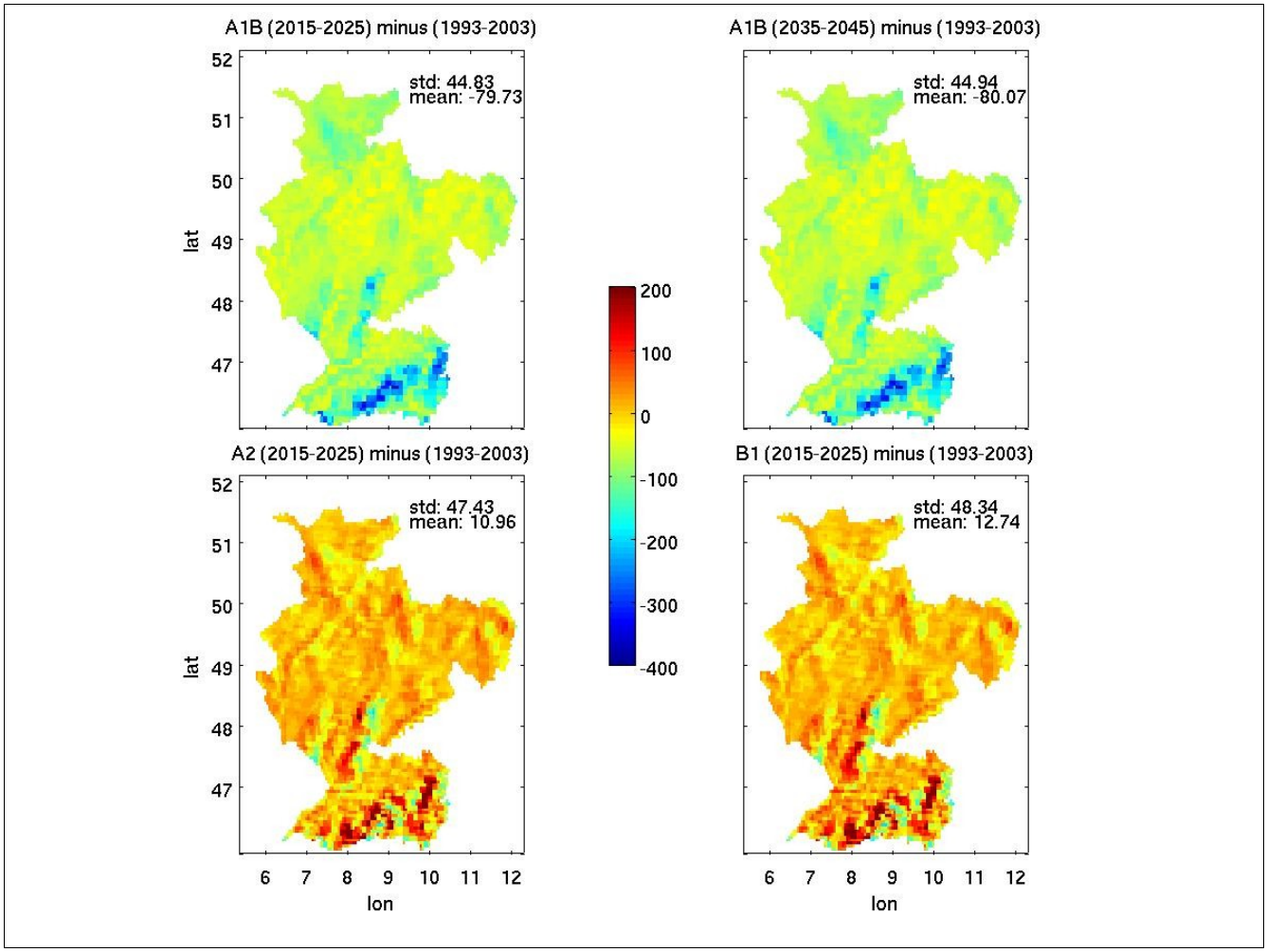

Figure 6. Difference in precipitation between climate scenarios and current situation for spring.

In the summer (Figure 7), scenario A1B receives less precipitation than the current situation. The largest differences can be found in the Alps. Also the variation in differences is the largest in this area. Both periods of scenario A1B show comparable results when looked at the mean and standard deviation. For scenario A2 and scenario B1, the difference is positive, which means that there will be more precipitation than in the current situation. The average precipitation difference for scenario B1 is higher than the average precipitation difference for scenario A2. Also the standard deviation for scenario B1 is higher when compared with scenario A2.

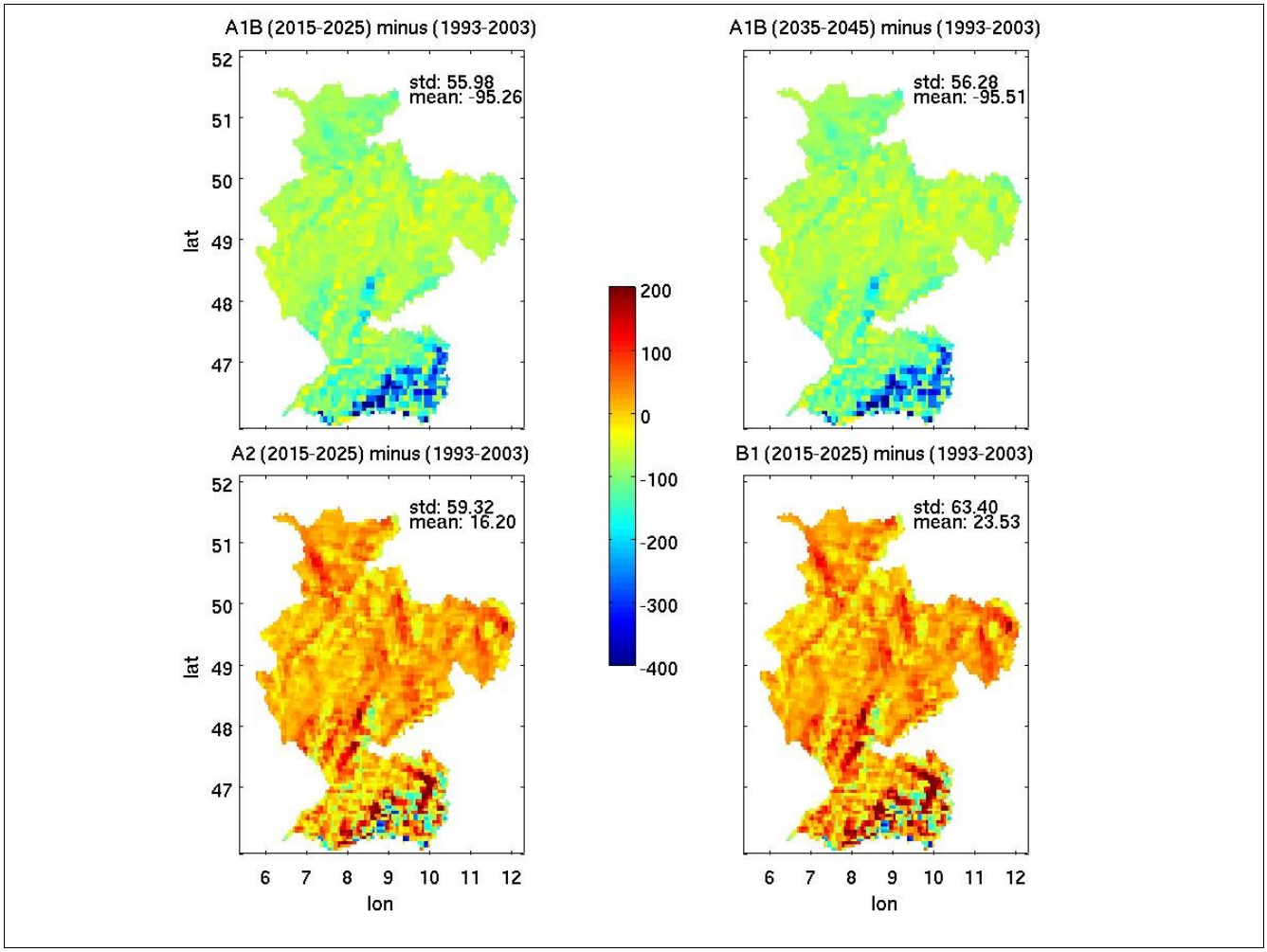

Figure 7. Difference in precipitation between climate scenarios and current situation for summer.

Figure 8 represents the difference in precipitation between the different scenarios and the current situation for autumn. The amount of precipitation for scenario A1B is smaller than the amount of precipitation in the current situation for both periods. Again, the largest difference in precipitation can be found in the Alps, this is also the area with the largest variability in differences. Both periods of scenario A1B have a similar average and standard deviation. The scenarios A2 and B1 both show an increase in precipitation when compared with the current situation. However, the increase of scenario B1 is slightly larger than the increase of scenario A2. This can be seen when looked at the mean precipitation differences of both scenarios. The scenarios A2 and B1 have a comparable standard deviation.

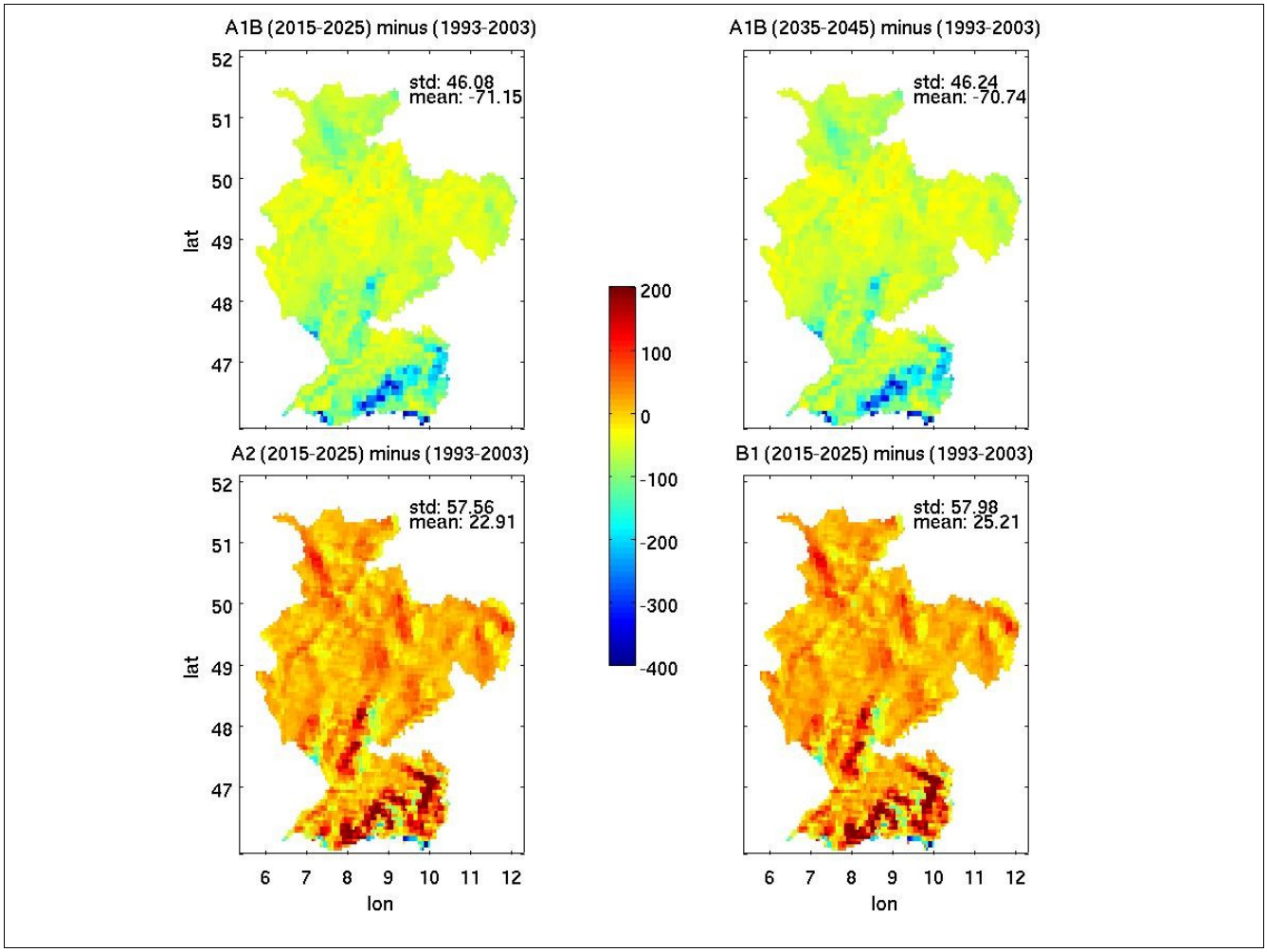

Figure 8. Difference in precipitation between climate scenarios and current situation for autumn.

Temperature analysis

Similar to Figures 5 through 8, Figures 9 through 12 represent differences between the different scenarios and the current situation, but now for temperature. Again, in the top right of each figure, the mean and standard deviation of the grid cells are plotted.

For the winter period (Figure 9), the upper left figure shows both a decrease and an increase of temperature when compared with the current situation. An increase in temperature will cover most of the Rhine Basin. The average temperature difference for the period 2015-2025 is 0.38 degrees. The second period of scenario A1B (upper right figure), has an even larger increase in temperature. The average temperature difference now is 1.58 degrees. The largest variation in temperature differences can be found in the Alps. This holds for all scenarios. When comparing the 2015-2025 period of the three scenarios with the current situation, all scenarios show an increase in temperature. Scenario B1 shows the largest increase in temperature and scenario A1B the smallest increase in temperature. The standard deviations of all scenarios do not differ much from each other.

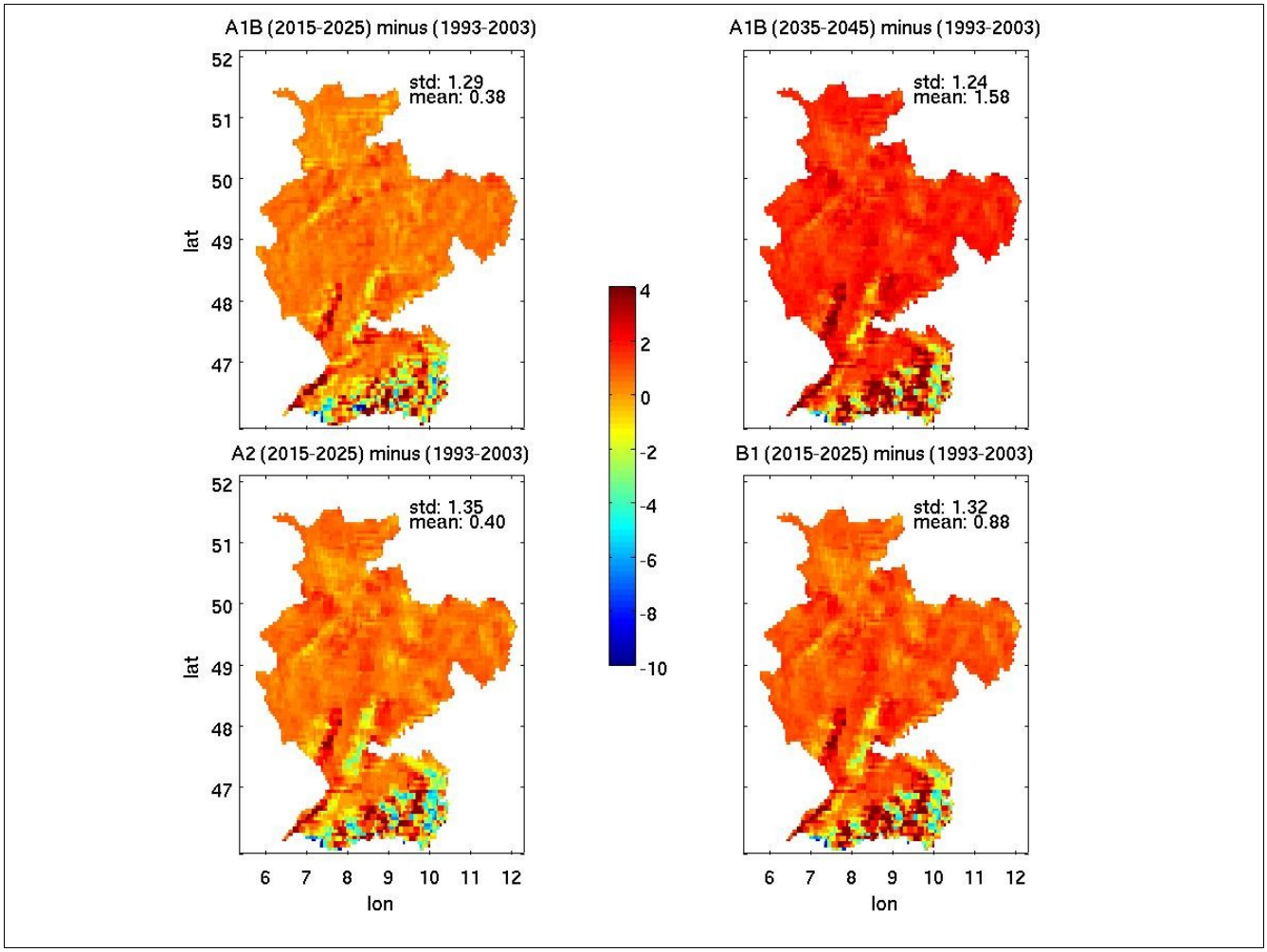

Figure 9. Difference in temperature between climate scenarios and current situation for winter.

Also in for spring (Figure 10), the largest variability in temperature differences can be found in the Alps. All the scenarios show both increases and decreases in temperature for this area. The period 2015-2025 for all three scenarios shows a decrease in temperature for the largest area of the Rhine Basin. Scenario B1 encounters the smallest decrease in temperature, whereas A1B shows the largest decrease. The standard deviations for all scenarios are quite similar. The second period of scenario A1B shows an increase in temperature for most of the Rhine Basin when compared to the current situation. The average temperature difference is 0.3 degrees. The standard deviation has decreased when compared with the previous period.

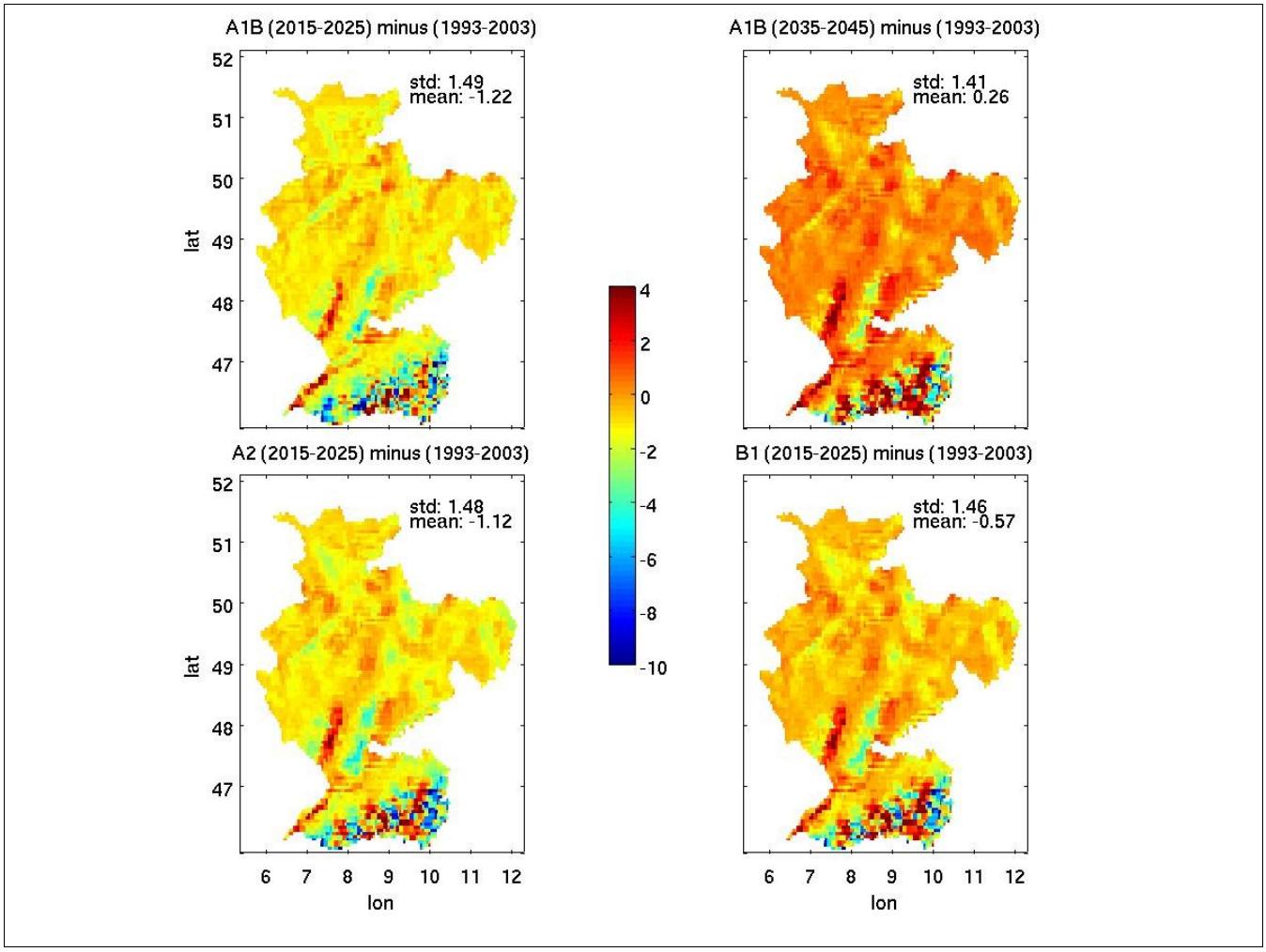

Figure 10. Difference in temperature between climate scenarios and current situation for spring.

Figure 11 represents the difference in temperature between the different scenarios and the current situation for summer. Again, the largest variability in temperature differences can be found in the Alps. All the scenarios show both increases and decreases in temperature for this area. The difference in temperature for all scenarios compared with the current situation is negative for most of the Rhine Basin. All average temperature differences are negative which indicates a decrease in temperature for all scenarios. Scenario A2 and B1 are quite comparable; they nearly have the same mean and standard deviation. The decrease in temperature for these scenarios is larger than the decrease in temperature for scenario A1B. However, the second period of scenario A1B shows an increase in temperature over larger areas in the Rhine Basin.

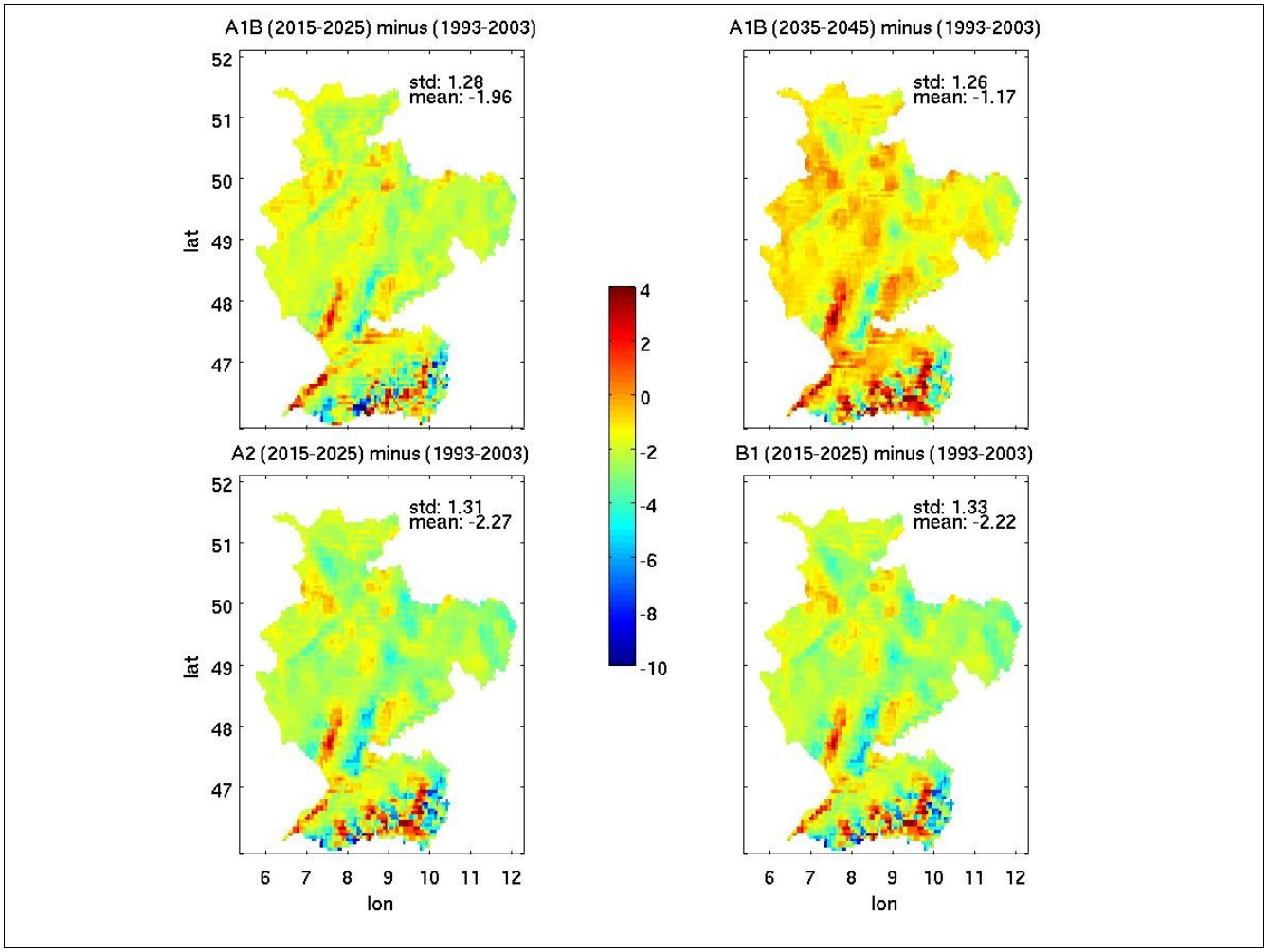

Figure 11. Difference in temperature between climate scenarios and current situation for summer.

In autumn (Figure 12), again, the largest variability in temperature differences can be found in the Alps. All the scenarios show both an increase and decrease in temperature for this area, where for scenarios A2 and B1 this is true in most of the Rhine basin. However, the average temperature difference for these two scenarios is negative, which means that the temperature is decreasing over the largest part of the Rhine Basin for these scenarios. Scenario A2 is decreasing the most. Scenario A1B reaches the highest temperature when compared with the current situation. The average temperature difference for this scenario is 0.3 degrees for 2015-2025 and 0.9 degrees for 2035-2045. It can be concluded that the temperature for this scenario continues to rise in the period after 2025. The standard deviations of all scenarios are almost similar to each other.

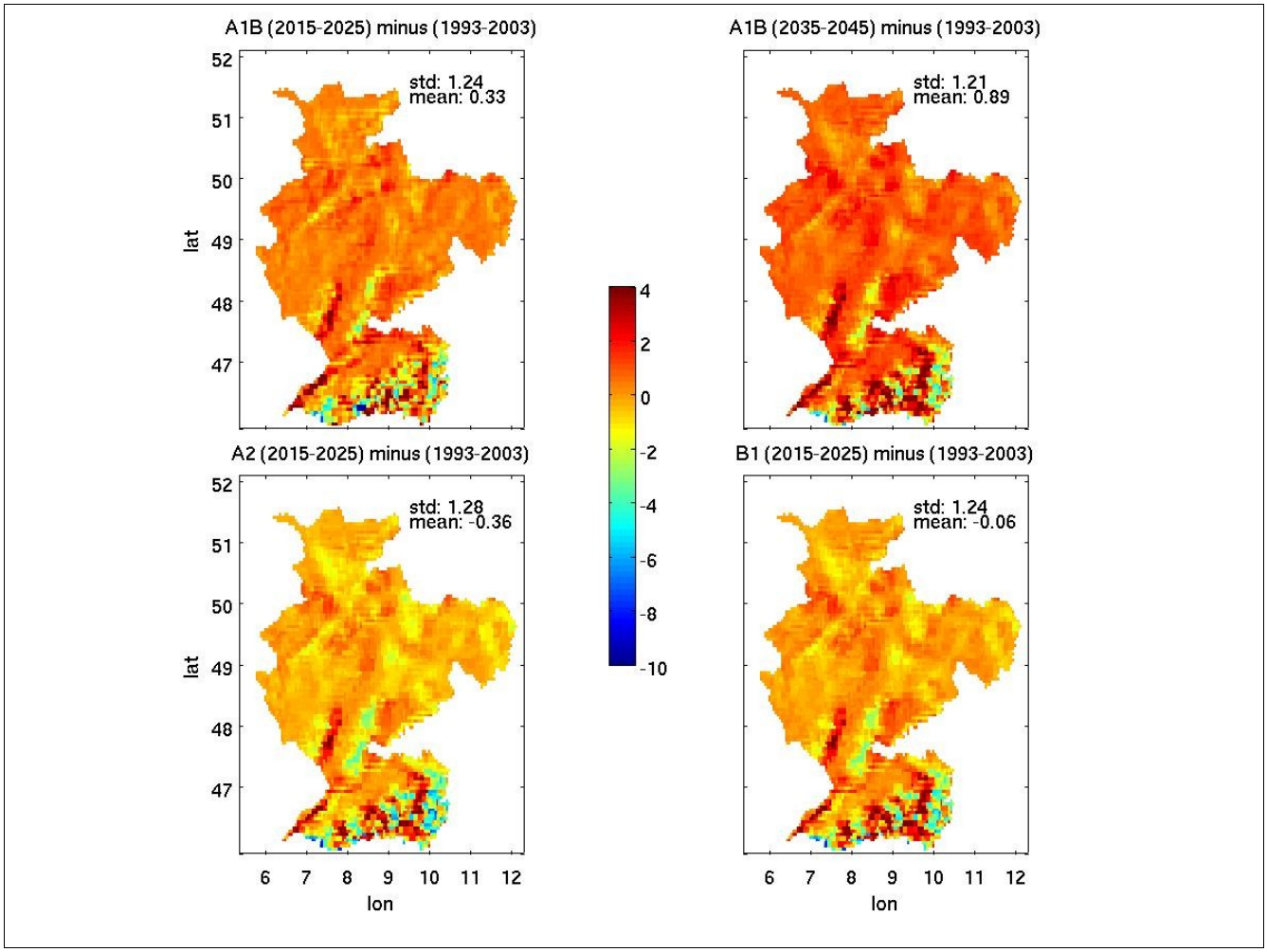

Figure 12. Difference in temperature between climate scenarios and current situation for autumn.

4. Model calibration

To calibrate VIC, seven parameters influencing the shape of the hydrograph and the total outflow volume were subjected to a sensitivity analysis. Based on this analysis, the depth of the (very thin) upper layer and the baseflow parameter W_s (see Figure 5) appeared to have no influence on the resulting hydrograph and were therefore left out of the calibration procedure to save computation time. Parameters influencing potential evapotranspiration, differing per vegetation type, were left at their default values. The resulting parameters for optimization are, similar to former applications [Lohmann et al., 1998a; Liang et al.,1994]: D_m and D_s to define the relation between baseflow and soil moisture in the lowest layer (see Figure 5), the shape parameter β in Eq. 1 and the depths of the lower two layers d_2 and d_3. Because these parameters are not transferable between the full and energy modes, VIC was re-calibrated for the water balance mode, using the same parameters. For optimizing the objective function O a power transformation was used to balance sensitivity to peak flows and low flows. The objective function can be written as:

$$O = \frac{1}{N}\sum_{i=1}^{N}\frac{(Q_{obs}^{\lambda} - Q_{sim}^{\lambda})}{\lambda} \qquad (2)$$

where N is the number of time steps and Q_{obs} and Q_{sim} are observed and simulated discharge respectively. Both are raised to the power λ which is taken as 0.3 in this study because this gives an optimal balance between sensitivity to peak and low flows [Misirli et al., 2003].

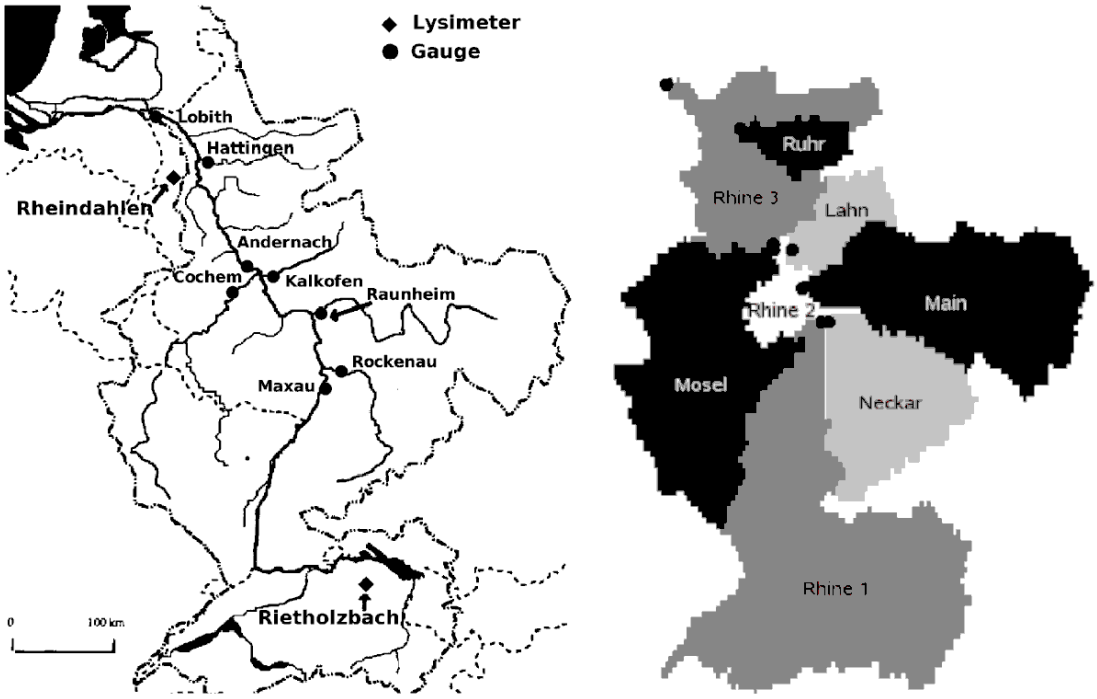

Figure 13. Location of the measuring gauges and lysimeters to verify the performance of the model (left), and the discretisation of the main sub-basins in VIC

(right).

The calibration routine was carried out for each of 7 areas separately, i.e., the five tributaries shown in Table 2, the Rhine upstream of Maxau and the Rhine between Maxau and Lobith. See also Figure 3. Ideally, the model would be calibrated in a fully distributed manner, i.e., with the possibility to assign parameter values to each individual grid cell, but this is not feasible in terms of computation time. By calibrating on individual sub-basins, different characteristics of the landscape can be treated differently. For example, the Alpine terrain is located in the area upstream of Maxau, the Schwarzwald area is located in the Mosel sub-basin, while the flatter areas are located more downstream.

Table 2. Tributaries of the Rhine basin and their characteristics. Mean, maximum and mean annual maximum discharge are calculated over the period 1993-2003. Same numbers are also shown for the basin outlet Lobith.

Tributary	**Gauge**	**Contributing area [km^2]**	**Mean discharge [m^{3}s^{-1}]**	**Maximum discharge [m^{3}s^{-1}]**	**Mean annual maximum discharge [m^{3}s^{-1}]**
Lahn	Kalkofen	5.304	48	587	394
Main	Raunheim	24.764	187	1991	1177
Mosel	Cochem	27.088	364	4009	2650
Neckar	Rockenau	12.710	154	2105	1396
Ruhr	Hattingen	4.118	75	867	611
Rhine	Lobith	185.000	2395	11775	8340

Because, as is described in the previous section, the model can be applied in two modes, being the water balance and the energy balance mode, the model was calibrated twice. In the water balance mode, the timestep is typically 1 day because there is no need to take into account the diurnal cycle, as there is in the full energy balance mode. Therefore, parameters cannot be transferred directly. The calibration period was selected from 1-10-1993 to 31-12-1994, where for each run the model was initialized using the period 1-1-1993 to 30-9-2009. Timeseries of observed and simulated discharge can be found in Figure 4. Also Nash-Sutcliffe model efficiencies (NS; Nash and Sutcliffe, 1970) are displayed. After calibrating the model, the remainder of the available data, i.e., from 1-1-1995 to 31-12-2003, is used for validation. Table 3 shows correlation coefficients, Nash-Sutcliffe efficiencies and relative volume errors for both the calibration and validation period.

Figure 4 and Table 3 show results for both the energy and water balance mode. Results in the calibration are slightly better for the water balance mode (e.g., NS is 0.56 for energy balance vs. 0.68 for water balance). In water balance mode, less physics is involved and the model is more sensitive to parameter settings and therefore easier to calibrate. A large part of the uncertainties are coming from the atmospheric data, which is slightly different from observations. This was already described in the previous section, see for more information Hurkmans et al., 2008. Therefore, the simulation in energy balance mode is repeated, but now precipitation is replaced by CHR precipitation (without recalibrating the model). Results are also shown in Figure 4 and Table 3. Results improve quite significantly using observed precipitation, for example NS jumps from 0.56 to 0.70 with CHR precipitation. All

performance indicators shown here are at a daily base, which is of course relevant for extreme peak flows, but it also explains the relatively low modeling efficiencies. When aggregated to for example 10 days (as was done in Hurkmans et al., (2008)) to remove routing effects, the efficiencies and correlations increase considerably.

The best results are reached at the basin outlet, Andernach and Lobith, because they integrate all processes occurring in the basin. The basin outlet is also the most interesting for climate assessments because they represent the main branch and the largest area. From the other stations, it appears that especially the Alpine part (upstream of Maxau) is poorly simulated, mainly because of three reasons: there are some large surface reservoirs in the area (e.g. the Bodensee, the largest lake in Europe) which are not (yet) represented in the model. Flood peaks can, therefore, be exaggerated in the simulations. Second, no snow pack data was available to specifically calibrate the snow submodel, leading to possible overestimation of snow melt. Third, differences in precipitation between ERA15 and CHR are concentrated mainly in the Alpine part. Indeed, especially the correlation coefficient of the calibration period increases drastically (from 0.66 to 0.81) for Maxau when CHR precipitation is used. For a more extensive discussion about these issues, see Hurkmans et al., 2008.

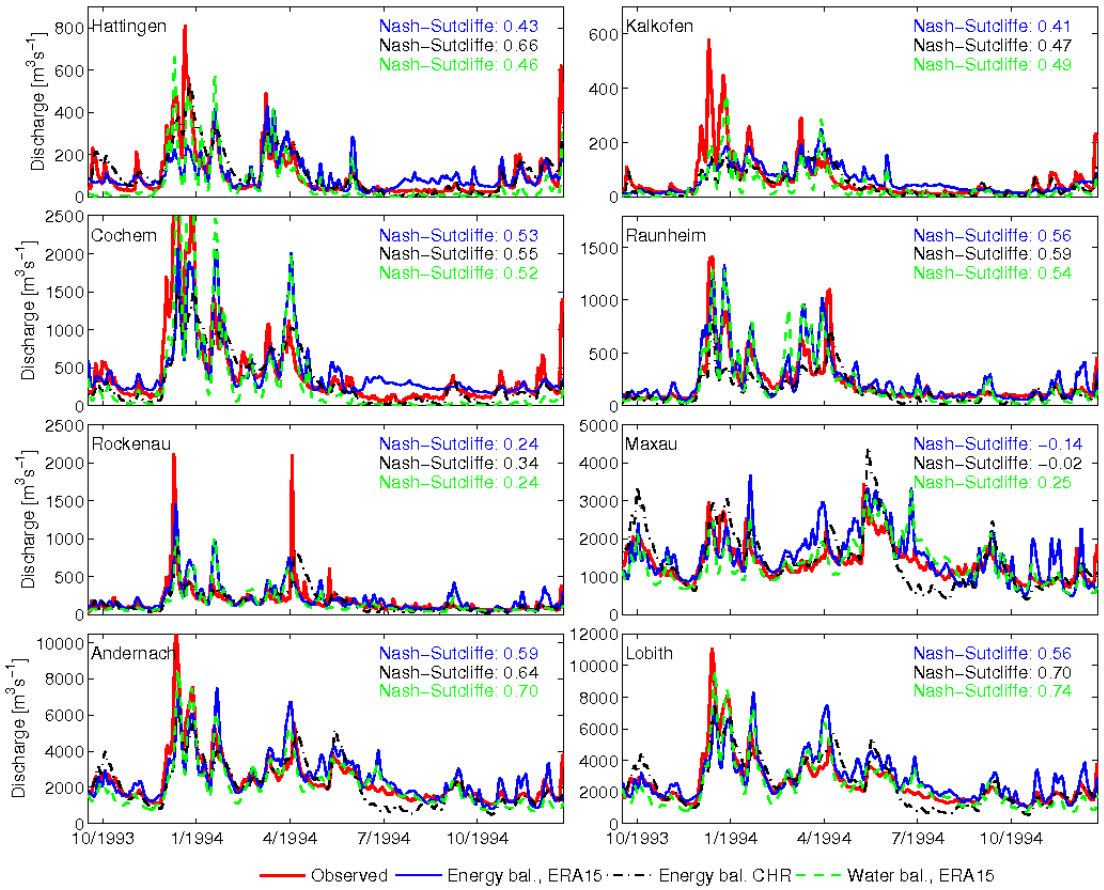

Figure 14. Timeseries of simulated and observed discharge over the calibration period (1-10-1993 – 31-12-1994) for the eight gauging stations in the basin (see Figure 3 for locations). Simulated discharge for the energy balance and the water balance modes are shown, as well as results of the energy balance model, but forced with observed (CHR) precipitation.

Table 3. Correlation coefficients, Nash-Sutcliffe model efficiencies and relative volume errors for three VIC simulations: energy balance (EB) and water balance (WB) modes, where EB is also shown as forced with CHR precipitation (EBchr). All indicators are shown for eight gauging stations in the basin, for both the calibration and validation period. Note that the simulation with CHR precipitation is not available after 1995, therefore, no information is shown for the validation period for CHR precipitation.

Calibration period	**Correlation coeff. [-]**			**Nash-Sutcliffe [-]**			**Rel. Vol. error [%]**		
Gauge	**EB**	**EBchr**	**WB**	**EB**	**EBchr**	**WB**	**EB**	**EBchr**	**WB**
Hattingen	0.65	0.83	0.76	0.43	0.66	0.46	0.59	11.5	-37.2
Kalkofen	0.64	0.74	0.78	0.41	0.47	0.49	-3.01	-28.7	-41.4
Cochem	0.73	0.77	0.84	0.52	0.55	0.52	-0.01	-22.1	-25.0
Raunheim	0.82	0.86	0.81	0.56	0.59	0.54	17.3	-31.5	-3.15
Rockenau	0.60	0.62	0.56	0.24	0.34	0.24	17.0	-4.75	-14.1
Maxau	0.66	0.81	0.71	-0.14	-0.02	0.25	12.2	5.35	-0.94
Andernach	0.78	0.83	0.87	0.59	0.64	0.70	4.71	-9.45	12.4
Lobith	0.78	0.85	0.89	0.56	0.70	0.74	10.6	-1.97	-8.72
Validation period									
Gauge									
Hattingen	0.66	-	0.65	0.44	-	0.21	5.83	-	-44.2
Kalkofen	0.58	-	0.68	0.33	-	0.30	-7.66	-	-48.8
Cochem	0.66	-	0.70	0.40	-	0.28	-7.91	-	-47.6
Raunheim	0.73	-	0.61	0.43	-	0.19	-11.0	-	-42.8
Rockenau	0.60	-	0.52	-0.55	-	0.06	3.49	-	-34.6
Maxau	0.55	-	0.51	-0.77	-	-0.35	15.5	-	-1.33
Andernach	0.63	-	0.58	0.24	-	0.16	4.16	-	-19.8
Lobith	0.69	-	0.64	0.33	-	0.24	8.73	-	-20.3

5. Model operation

Below, in sections 5.1 and 5.2, the application of the VIC model combined with the routing algorithm to the Rhine basin is described in detail. All input and parameter files that are provided here, solely apply to the Rhine basin. Of course, it is possible to apply the model to other areas, such as the other NeWater case study areas. General instructions as to how to set-up and apply the model are on the VIC website (see the link in section 5.1), but in paragraph 5.3 a summary is provided of the required data and preprocessing steps.

5.1. VIC

The VIC model is programmed in C. For modifications, the source code should be altered. The source code is included in the archive file, or can be downloaded from: http://www.hydro.washington.edu/Lettenmaier/Models/VIC/VIChome.html. After modifying the source code, it needs to be recompiled by issuing the commands

"make clean" and "make" in the source directory at the command prompt.

The executable is called 'vicNl' and can be executed from the command prompt in any UNIX system by issuing the following command: "./vicNl -g <config-file>". For windows, other libraries are required preventing VIC from running under Windows. The model requires several input files, which all depend on the type of application. In this setup, the model is equipped for simulation of the fully coupled water - and energy balance at a temporal resolution of 3 hours and a spatial resolution of 0.05 degree (approx. 5km) on a regular latitude-longitude grid. The required inputfiles are:

- <config-file>: a global configuration file containing global parameters en paths to other input and output files
- vegetation parameter file: land use types for every pixel
- vegetation library file: vegetation parameters for every land use type
- soil parameter file: soil parameters en coordinates for every grid cell1
- snow elevation band file: elevation zones within every grid cell
- atmospheric data files: atmospheric forcing data. One file is needed for every grid cell (approx. 7800) in the basin. Every file contains one row for every timestep and one column for each of seven variables:
    - 3 hour accumulated precipitation [mm]
    - average 2m temperature [Celsius]
    - surface air pressure [kPa]
    - surface vapor pressure [kPa]
    - shortwave incoming radiation [Wm^{-2}]
    - longwave incoming radiation [Wm^{-2}]
    - wind speed [ms^{-1}]

The model runs for each grid cell separately, so all time steps are simulated for one cell before moving on to the next cell. This implies that one input and one outputfile (containing all timesteps) are required for each pixel. Because most atmospheric forcing datasets are organized in one file per time step, this is an extra reason for preprocessing atmospheric data (see section 3.2). The soil parameter file determines the grid cells to be simulated; it contains all cell coordinates (from which the filename for the input and output file follows), and each cell can be 'activated' by setting the first integer value in every row of the soil parameter file to 1 (instead of 0). In this setup, all cells that are located within the basin boundaries are activated. It is also possible to run the model for each sub-basin separately, in this case run the 'create_soilfile.c' program in the prepare_soilfile directory to create a soil parameter file where the proper cells are activated. To select a sub-basin, change the value in the flag.txt file as follows.

1. Ruhr (Hattingen)
2. Lahn (Kalkofen)
3. Neckar (Rockenau)
4. Mosel (Cochem)
5. Main (Raunheim)
6. Upstream Maxau (Maxau)
7. Total basin (Lobith)

By default, the model runs at a 3-hourly timestep. If integration on daily base is desired (which greatly reduces simulation time), the energy balance cannot be solved and a different set of parameters is required. Calibrated parameters are also provided

(in the preparare_soilfile directory). However, these parameter values need to be implemented in the soil parameter file. By means of the create_soilfile script a correct soil parameter file can be created; in this case the paths to the parameter files need to be changed from 'parameters_energybalance', to 'parameters_waterbalance'. In addition, in the config_inputfile, the timestep needs to be changed from '3' to '24' at the designated locations. Finally, all atmospheric data (from REMO) need to be integrated to daily values. For this end, a matlab script 'aggregate_VICforcing_3hourly2daily.m' is included in the 'preprocess' directory. Finally, all practical information about VIC, the content of all input and output files etcetera is well documented at the website mentioned before, which is also included in the included archive file.

5.2 Routing model

After the VIC simulation is completed, the routing algorithm (for the specific sub-basin or, in case the entire Rhine basin is desired, all sub-basins) needs to be run separately afterwards.
The routing model is programmed in Fortran 77. The source code is included in the archive file, and can also be downloaded from the VIC website. Note that the executable that is included here is modified to allow for (3-hourly) VIC output files. For daily output, the OPTI parameter in the "make_convolution.f" file should be altered (and the routing algorithm recompiled). The resulting executable is called "./rout" and can be executed from the command prompt. If the source code is changed, recompile using "make clean" and "make". The routing model requires several input and configuration files.

- rhine.inp: contains general parameters and paths to in- and output files.
- Flow direction file: map of flow directions (integers representing the direction of flow for each pixel; 1 for north, 2 for north-east, 3 for east etc…until 8 for north-west.)
- fraction file: for large scales, pixels at the edges of the basin are only partially inside the basin. This file contains these fractions for cells on the edge.
- Stations file: row/column coordinates (in flow direction map) of the measuring gauges for which a simulated hydrograph is desired.
- Xmask file: length in meters of the channel network through a specific pixel – depends on flow direction.
- Unit hydrograph file: unit hydrograph of flow within the pixel to the channel network. Because in this application the resolution is relatively high (and the pixels, therefore, small) is its influence negligible.

5.3 Application to other areas

As was mentioned in section 5.1, VIC requires the following parameter files:

- soil parameter file
- vegetation parameter file
- vegetation library file
- elevation band file
- forcing data files (for every pixel)

Each of those files (except for the vegetation library) needs to be created specifically for the river basin the model is applied to. In the folder 'preprocessing_other_areas', some scripts are provided to construct files in the correct format from data that needs to be downloaded. Sources to download data from are indicated below. Note that geographic projections of the data vary between data sources and areas of the world. For further preprocessing, all data should be re-projected to a regular latitude-longitude system with datum WGS84 (i.e., no projection), and if possible cropped to the area of interest to prevent processing of enormous data files.

Soil parameter file
For the soil parameter file, spatial information about soil types is required. Soil classification is based on the global FAO sand and clay fraction datasets (Reynolds et al., 1999), which can be downloaded at the following website:
http://www.ngdc.noaa.gov/seg/cdroms/reynolds/reynolds/reynolds.htm

Furthermore, the snow elevation band file needs to be prepared (see below), and parameters are read from the soil.txt library (which is also in the folder "preprocessing_other_areas". The file that is obtained contains the default calibration parameter settings, these have to be overwritten with calibration results as is described in section 5.1.

Vegetation parameter file and vegetation library file
Creation of this file is highly dependent on what kind of land cover database is used. Scripts that are included in the folder 'preprocessing_other_areas' are based on the European PELCOM database
(http://www.geo-informatie.nl/projects/pelcom/download/folder.pdf)

However, if the basin under consideration is not in Europe also a global dataset is available at:
http://www.geog.umd.edu/landcover/1km-map.html

The creation of the vegetation parameter file occurs in two steps, first the fractions of land cover types in each modeling pixel is calculated. Note that the vegetation parameter library file needs to be adjusted to include the correct land use types when different land cover products are used because they are usually different.

Elevation band file.
This file contains, for every grid cell, information about distribution of elevation within each of those grid cells. If elevations differs significantly within pixels, dividing pixels into zones, each with their own mean elevation and areal fraction, improves evaporation and snow melt parameterizations.
The file is essentially created by the elevband.c script (included in the folder 'preprocessing_other_areas'). This script, though, needs digital elevation data at a higher resolution than the model is intended to run. Global digital terrain data at a resolution of 1 km can be downloaded at:
http://eros.usgs.gov/products/elevation/gtopo30/hydro/index.html

Additionally, the eleband-script needs size and coordinates of all cells in the modelling domain. The matlab script 'create_dummy_for_elevband.m' provides these.

Atmospheric forcing files

In this case we assume that climate scenarios from MPI-M are available through NeWater, in which case the preprocessing should be similar to what is described in section 3.2. If not, preprocessing highly depends on the format of the source data. The goal however, should be one file for each grid box in the model, all containing one row for each time step (usually three hours) and a column for every variable. At minimum, the required variables are daily precipitation and daily maximum and minimum temperature. If the time step is 3 hours, only 3 hourly precipitation and temperature is required. However, if additional data (humidity, pressure, radiation, wind speed) is available it can be used as well.

Routing
Most of the parameter files needed for the routing algorithm are derived from digital elevation information, for instance the Hydro_1K data (see "Elevation band file" in the previous section). Derivation of the flow direction files and fraction files from this elevation data is explained in detail at:
http://www.hydro.washington.edu/Lettenmaier/Models/VIC/Documentation/Bernt/rout/mainframe_rout1.htm
For the generation of the flow network, several scripts are needed, as is described on the website. The scripts are included in the folder
"preprocessing_other_areas/routing/". The folder also contains a "create_xmask.c" script, which is needed to create the Xmask file (see previous section) from the flow direction file.

6. References

Brooks, R. H., and A. T. Corey (1964), Hydraulic properties of porous media, Clorado State University, Fort Collins, USA.

Jacob, D. (2001), A note to the simulation of the annual and inter-annual variability of the water budget over the Baltic Sea drainage basin, Meteorol. Atmos. Phys., 77, 61–73.

Hurkmans, R. T. W. L., H. de Moel, J. C. J. H. Aerts, and P. A. Troch (2008), Water balance versus land surface model in the simulation of Rhine river discharges, Water Resour. Res., 44, W01418, doi:10.1029/2007WR006168

Liang, X., D. P. Lettenmaier, E. F. Wood, and S. J. Burges (1994), A simple hydrologically based model of land surface water and energy fluxes for general circulation models, J. Geophys. Res., 99(D7), 14,415–14,458.

Liang, X., and Z. Xie (2001), A new surface runoff parameterization with subgrid-scale soil heterogeneity for land surface models, Adv. Water Resour., 24, S0309-1708(01)00021-X.

Lohmann, D., R. Nolte-Holube, and E. Raschke (1996), A large-scale horizontal routing model to be coupled to land surface parameterization schemes, Tellus, 48A, 708–721.

Lohmann, D., E. Raschke, B. Nijssen, and D. P. Lettenmaier (1998a), Regional scale hydrology: I. Application of the VIC-2L model coupled to a routing model, Hydrolog. Sci. J., 43(1), 131–141.

Lohmann, D., E. Raschke, B. Nijssen, and D. P. Lettenmaier(1998b), Regional scale hydrology: II. Application of the VIC-2L model to the Weser river, Germany, Hydrolog. Sci. J.,43(1), 143–158.

Lohmann, D., K. E. MItchell, P. R. Houser, E. F. Wood, J. C.Schaake, A. Robock, B. A. Cosgrove, J. Sheffield, Q. Duan, L. Luo, W. Higgins, R. T. Pinker, and J. D. Tarpley (2004b), Streamflow and water balance intercomparisons of four land surface models in the North American Land Data Assimilation System project, J. Geophys. Res., 109, D07S91, doi:10.1029/2003JD003517

Misirli, F., H. V. Gupta, S. Sorooshian, and M. Thiermann(2003), Bayesian recursive estimation of parameter and output uncertainty for watershed models., in calibration of watershed models, vol. 6, edited by Q. D. et al., pp. 113–124, American Geophysical Union, Washington DC.

Mucher, S., K. Steinnocher, J.-L. Champeaux, S. Griguolo,K. Wester, C. Heunks, and V. van Katwijk (2001), Establishment of a 1-km Pan-European Land Cover database for environmental monitoring, ISPRS, 33.

Nash, J. E., and I. V. Sutcliffe (1970), River flow forecasting through conceptual models. Part I - a discussion of principles, J. Hydrol., 10, 282–290.

Nijssen, B., D. P. Lettenmaier, X. Liang, S. W. Wetzel, and E. F. Wood (1997), streamflow simulation for continental-scale river basins, Water Resour. Res., 33(4), 711–724.

Nijssen, B., G. M. O'Donnell, D. P. Lettenmaier, D. Lohmann, and E. F. Wood (2001), Predicting the discharge of global rivers, J. Climate, 14, 3307–3323.

Reynolds, C. A., T. J. Jackson, and W. J. Rawls (2000), Estimating water-holding capacities by linking the Food and Agriculture Organization soil map of the world with global pedon databases and continuous pedotransfer functions, Water Resour. Res., 36(12), 3653–3662.

Sprokkereef, E. (2001b), Eine hydrologische Datenbank f¨ur das Rheingebiet, International Commission for the Hydrology of the Rhine basin (CHR).

Todini, E. (1996), The ARNO rainfall-runoff model, J. Hydrol., 175, 339–382, S0022-1694(95)02853-6.

Wood, A. W., A. Kumar, and D. P. Lettenmaier (2005), A retrospective assessment of National Centers for Environmental Prediction climate model-based ensemble hydrologic forecasting in the western United States, J. Geophys. Res., 110, D04105, doi:10.1029/2004JD004508.